

AUGUST 23 2023

High-resolution frequency-difference beamforming for a short linear array

Xueli Sheng; Chaoping Dong; Longxiang Guo  ; Xin Wang

 Check for updates

J. Acoust. Soc. Am. 154, 1191–1201 (2023)

<https://doi.org/10.1121/10.0020722>



View
Online



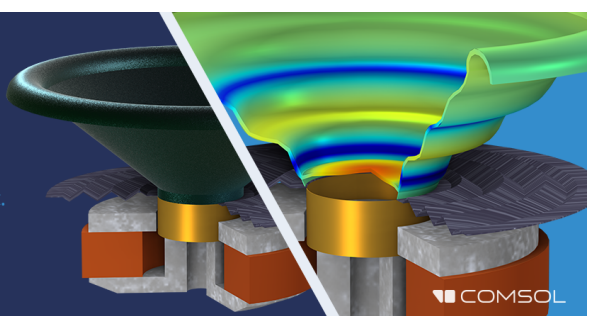
Export
Citation

CrossMark

Take the Lead in Acoustics

The ability to account for coupled physics phenomena lets you predict, optimize, and virtually test a design under real-world conditions – even before a first prototype is built.

» Learn more about COMSOL Multiphysics®



COMSOL

High-resolution frequency-difference beamforming for a short linear array

Xueli Sheng,¹ Chaoping Dong,¹ Longxiang Guo,^{2,a)}  and Xin Wang³

¹Acoustic Science and Technology Laboratory, Harbin Engineering University, Harbin 150001, China

²Key Laboratory of Marine Information Acquisition and Security, Ministry of Industry and Information Technology, Harbin Engineering University, Harbin 150001, China

³College of Underwater Acoustic Engineering, Harbin Engineering University, Harbin 150001, China

ABSTRACT:

Conventional beamforming (CBF) is a commonly employed approach for detecting and estimating the direction-of-arrival (DOA) of acoustic signals in underwater environments. However, CBF becomes ambiguous due to spatial aliasing when the received signal's half wavelength is smaller than the array spacing. Frequency-difference beamforming (FDB) allows for processing data in the lower frequency Δf without encountering spatial aliasing by utilizing the product of array data at frequency f with its complex conjugate at frequency $f + \Delta f$. However, lower frequency results in a wider mainlobe, which can lead to poorer DOA performance for short arrays. In this paper, a fourth-order cumulants FDB method and a conjugate augmented FDB method are proposed to extend an M -element uniform linear array to $2M - 1$ and $4M - 3$ elements. The proposed methods generate narrower beams and lower sidelobe levels than the original FDB for short arrays with large spacing. And by setting the signal subspace dimension reasonably, the proposed methods can improve the weak target detection ability under strong interference compared with FDB. Last, we verify the excellent performance of the proposed methods through simulations and experimental data. © 2023 Acoustical Society of America. <https://doi.org/10.1121/10.0020722>

(Received 6 December 2022; revised 1 August 2023; accepted 2 August 2023; published online 23 August 2023)

[Editor: Zoi-Heleni Michalopoulou]

Pages: 1191–1201

I. INTRODUCTION

Conventional beamforming (CBF) is a widely used array processing method that can accurately estimate the direction of arrival (DOA) using a small number of samples and is robust to signal mismatch.¹ However, CBF becomes ineffective due to spatial aliasing when the array spacing is greater than half the wavelength of the received signal. Frequency-difference beamforming (FDB) method was proposed to address this issue.^{2,3} The FDB method generates a signal with a frequency of Δf by calculating the quadratic product of the frequency domain signal $X(f)^*X(f + \Delta f)$ (where * represents conjugate). This transforms the signal frequency from out-of-band to in-band, shifts the beamformer to a lower frequency, and eliminates the spatial aliasing components. The excellent performance of FDB has been thoroughly analyzed⁴ and validated through experiments.⁵ Previous studies have also demonstrated the robustness of FDB in uncertain environments,^{6,7} and its enhanced method has been employed in sound source localization.^{8,9} However, the signal frequency decreases after frequency-difference processing, and the wider beam widths make it challenging to detect two targets within the same beam, particularly for a short linear array. In order to address this issue, this study proposes the utilization of the fourth-order-cumulants-based virtual aperture extension method to

enhance the DOA estimation performance of FDB in short linear arrays.

Several studies^{10,11} have achieved improved FDB resolution by utilizing multiple signal classification (MUSIC). The FDB-MUSIC can greatly decrease the main lobe width and the sidelobe level. The method's performance is closely related to the signal subspace dimension in DOA estimation of multi-targets for short arrays, and this feature will be demonstrated in Sec. III. Deconvolved conventional beamforming¹ (DCB) is a novel high-resolution approach which has been implemented in FDB¹² (Deconv-FDB). DCB can substantially enhance the resolution but may be susceptible to low signal-to-noise ratio (SNR) and inadequate array elements. Recently, compressed sensing^{13,14} has also been applied to FDB to improve spatial resolution in high SNR.¹⁵ Sparse array methods,^{16–20} and sparse Bayesian learning,^{21–23} among other high-resolution array processing techniques, have exhibited good performance but have not yet been utilized in FDB.

Virtual aperture expansion²⁴ is another practical high-resolution technique. The frequently employed virtual aperture expansion approach is based on cumulants. Cumulants can be utilized to construct virtual covariance matrices whose signal subspace can be characterized by an expanded aperture. Although not all of the elements that create the effective aperture are physically present, the covariance matrix can still be computed and utilized in a direction-finding algorithm. By using the fourth-order cumulants (Cum4), Gaussian noise can be suppressed while expanding

^{a)}Also at Acoustic Science and Technology Laboratory, Harbin Engineering University, Harbin 150001, China. Email: heu503@hrbeu.edu.cn

the array aperture to attain high resolution.^{24,25} Shan *et al.*²⁶ proposed a conjugate augmented (CA) method that employs the second-order statistics of the received signals to obtain the conjugate steering matrix. The conjugate steering matrix is utilized in conjunction with the steering matrix to determine the Cum4. This combination of second-order statistics and Cum4 can suppress not only Gaussian noise but also non-Gaussian noise.²⁷

As the Cum4 can increase resolution via virtual aperture expansion and has the potential to suppress noise, we believe that combining FDB with Cum4 virtual aperture expansion is an ideal approach for high-resolution FDB with large-spacing short arrays. Therefore, we present two methods that combine FDB with Cum4 and CA in this paper. Both methods, Cum4-FDB and CA-FDB, are founded on Cum4 and can expand M -element uniform arrays to $2M - 1$ and $4M - 3$ elements, respectively. Although the Cum4-based approach is computationally intensive, it is feasible for short arrays in this paper. We derived the signal model and analyzed the performance of the proposed algorithms. In comparison to the original FDB, these two methods exhibit improvements primarily in the following aspects:

- (1) Cum4-FDB and CA-FDB yield narrower main lobes and lower side lobe levels than FDB.
- (2) The CA methods can achieve higher angular resolution and exhibit superior performance under low SNR.
- (3) Cum4-FDB and CA-FDB can be combined with MUSIC (ML-FDB and CAM-FDB) for incoherent sound sources to achieve higher resolution. And by reasonably setting the signal subspace dimension, ML-FDB, and CAM-FDB can overcome the shortcomings of FDB and significantly improve the detection performance of weak targets in the presence of strong interference.
- (4) Experimental results demonstrate that Cum4-FDB and CA-FDB can be applied to coherent sources such as multi-path environments, and both can achieve superior performance to the original FDB.

This paper verifies the previously mentioned advantages through simulations and experimental data.

The paper is organized as follows. Sections II and III explain the original FDB and the implementation of virtual aperture extension techniques, respectively. Simulation studies are presented in Sec. IV, and Sec. V verifies the performance using two experimental cases. The limitations and issues are discussed in Sec. VI, and the conclusions are presented in Sec. VII.

Notations: We use thin characters to represent scalars and lower-case (upper-case) bold characters to denote vectors (matrices). $(\cdot)^*$ denotes a complex conjugate, $(\cdot)^H$ denotes a conjugate transpose, $(\cdot)^T$ denotes a transpose, and \otimes denotes a Kronecker product.

II. FORMULATIONS OF FREQUENCY-DIFFERENCE BEAMFORMING

References 2, 3, and 12 have provided a detailed description of the FDB derivation, and only the essential

results will be presented here. We consider a uniform linear array with M evenly spaced elements, and the spacing is d . The signal from a far-field point sound source is assumed to be incident in the form of a plane wave, and the sound speed is c . The signal frequency band is $[f_L, f_H]$. Then the frequency-difference autoprod⁶ ap of m -th element is defined by

$$ap_m(\Delta f, f) \equiv x_m^*(f)x_m(f + \Delta f), \quad (1)$$

where $x_m(f)$ is the frequency spectrum at frequency f of the received signal on the m -th element, Δf is a user-chosen difference frequency, $f_L \leq f \leq f_H - \Delta f$, $\Delta f \leq c/2d$. Then the beamformed output at the frequency f with difference frequency Δf can be expressed as

$$b_\Delta(\Delta f, f) = \left| \sum_{m=1}^M ap_m(\Delta f, f) \exp \left[\frac{-j2\pi\Delta f(m-1)d \sin \theta}{c} \right] \right|^2, \quad (2)$$

where θ is the scanning direction. Since the range for f is from f_L to $f_H - \Delta f$, $b_\Delta(\Delta f, f)$ can be incoherently averaged through the signal frequency bandwidths,

$$b_{\Delta wb} = \frac{1}{N_f} \sum_{f=f_L}^{f_H-\Delta f} b_\Delta(\Delta f, f), \quad (3)$$

where N_f represents the number of calculated $b_\Delta(\Delta f, f)$.

III. IMPLEMENTATION OF VIRTUAL APERTURE EXTENSION

A. Cum4-FDB

First, we derive the array signal model of Cum4-FDB. The frequency-difference autoprod⁶ of m -th element in Eq. (1) can be further expressed as

$$\begin{aligned} & x_m^*(f)x_m(f + \Delta f) \\ &= \left(n_m(f) + \sum_{l=1}^p a_m^l(f)s^l(f) \right)^* \\ &\quad \times \left(n_m(f + \Delta f) + \sum_{l=1}^p a_m^l(f + \Delta f)s^l(f + \Delta f) \right) \\ &= n_m^*(f)n_m(f + \Delta f) + n_m^*(f) \sum_{l=1}^p a_m^l(f + \Delta f)s^l(f + \Delta f) \\ &\quad + n_m(f + \Delta f) \sum_{l=1}^p (a_m^l(f)s^l(f))^* \\ &\quad + \sum_{l=1}^p \sum_{k=1}^p (a_m^l(f))^* a_m^k(f + \Delta f)(s^l(f))^* s^k(f + \Delta f), \end{aligned} \quad (4)$$

where s is the source signal spectrum, p is the source number, l and k are the source indices, n is the receiving noise spectrum, and $m = 1, 2, \dots, M$. $a_m^l(f)$ is defined as

$$a_m^l(f) = \exp\left[-\frac{j2\pi d(m-1)f \sin(\theta_l)}{c}\right], \quad (5)$$

where θ_l represents the incoming direction of l -th source signal. The first three terms in Eq. (4) together make up the noise of frequency-difference output. The last term in Eq. (4) is the signal term and can be further decomposed as

$$\begin{aligned} & \sum_{l=1}^p \sum_{k=1}^p (a_m^l(f))^* a_m^k(f + \Delta f) (s^l(f))^* s^k(f + \Delta f) \\ &= \sum_{l=1}^p a_m^l(f) (s^l(f))^* s^l(f + \Delta f) \\ & \quad + \sum_{l \neq k}^{p,p} (a_m^l(f))^* a_m^k(f + \Delta f) (s^l(f))^* s^k(f + \Delta f). \end{aligned} \quad (6)$$

In Eq. (6), the double sum over source paths has been separated into diagonal ($l = k$) and off diagonal ($l \neq k$) terms. The off diagonal terms are considered cross term interferences, which have limited influence according to the simulations and experimental results in this paper, therefore, ignored. The detailed nature and mitigation of cross term can be found in Refs. 28 and 29.

Frequency-difference processing is usually broadband, so we can obtain a sequence with a difference frequency of Δf ,

$$X_m = \left[x_m^*(f_1) x_m(f_1 + \Delta f), x_m^*(f_2) x_m(f_2 + \Delta f), \dots, x_m^*(f_{N_f}) x_m(f_{N_f} + \Delta f) \right]^T. \quad (7)$$

$f_1, f_2, \dots, f_{N_f} \in [f_L, f_H - \Delta f]$, and are determined by fast Fourier transform (FFT) points. Therefore, the broadband frequency-difference array signal of one frame data can be expressed as

$$X = AS + N, \quad (8)$$

where $X = [X_1, X_2, \dots, X_M]^T$. X_m has been defined in Eq. (7) and has removed the cross term interferences defined in Eq. (6). Other terms are defined as

$$A = [a^1, a^2, \dots, a^p],$$

$$a^l = \left[1, \exp\left\{-\frac{j2\pi d\Delta f \sin(\theta_l)}{c}\right\}, \dots, \exp\left\{-\frac{j2\pi d(M-1)\Delta f \sin(\theta_l)}{c}\right\} \right]^T, \quad l = 1, 2, \dots, p,$$

$$S = [S^1, S^2, \dots, S^p]^T,$$

$$S^l = \left[(s^l(f_1))^* s^l(f_1 + \Delta f), (s^l(f_2))^* s^l(f_2 + \Delta f), \dots, (s^l(f_{N_f}))^* s^l(f_{N_f} + \Delta f) \right]^T,$$

$$N = [N_1, N_2, \dots, N_M]^T,$$

$$N_m = [n_m(f_1, (f_1 + \Delta f)), n_m(f_2, (f_2 + \Delta f)), \dots,$$

$$n_m(f_{N_f}, (f_{N_f} + \Delta f))]^T,$$

$$n_m(f, (f + \Delta f))$$

$$= n_m^*(f) n_m(f + \Delta f) + n_m^*(f) \sum_{l=1}^p a_m^l(f + \Delta f) s^l(f + \Delta f) \\ + n_m(f + \Delta f) \sum_{l=1}^p (a_m^l(f))^* s^l(f). \quad (9)$$

$X \in \mathbb{C}^{M \times N_f}$, $A \in \mathbb{C}^{M \times p}$, $S \in \mathbb{C}^{p \times N_f}$ and $N \in \mathbb{C}^{M \times N_f}$ represent the receiving frequency-difference signal matrix, steering matrix, source frequency-difference signal matrix, and noise matrix, respectively. Equations (8) and (9) are the broadband array signal model of Cum4-FDB.

When dealing with real data, the receiving frequency-difference signal matrix X will be input to calculate the averaged Cum4 matrix

$$\begin{aligned} C &= E\left\{[X \otimes X^*][X \otimes X^*]^H\right\} \rightarrow M \times M \\ &\quad - E\{X \otimes X^*\}E\left\{[X \otimes X^*]^H\right\} - E\{XX^H\} \\ &\quad \otimes E\{[XX^H]^*\}, \end{aligned} \quad (10)$$

where $C \in \mathbb{C}^{M^2 \times M^2}$. The steering vector of Cum4-FDB after array aperture expansion is given by

$$\begin{aligned} a_{Cum4}(\theta) &= a(\theta) \otimes a^*(\theta), \\ a(\theta) &= \left[1, \exp\left\{-\frac{j2\pi d\Delta f \sin(\theta)}{c}\right\}, \dots, \exp\left\{-\frac{j2\pi d(M-1)\Delta f \sin(\theta)}{c}\right\} \right], \end{aligned} \quad (11)$$

where θ is the scanning direction. The length of $a_{cum4}(\theta)$ is M^2 . The DOA output of Cum4-FDB can be expressed as

$$P_{Cum4}(\theta) = \|a_{Cum4}(\theta)C\|_1^2, \quad M^2 \text{ in } M^2? \quad (12)$$

where $\|\cdot\|_1$ represent 1-norm (sum of absolute values) of the vector.

The Cum4-FDB method can be combined with MUSIC to achieve better performance for incoherent sources, called a MUSIC-like method.²⁶ As in the case of the MUSIC algorithm, we can compute the eigen decomposition of C . Its eigenvectors are separated into the signal and noise subspaces according to the eigenvalues. Let $E_n = \text{span}\{e_{D+1}, e_{D+2}, \dots, e_{M^2}\}$ be the noise subspace; then the spatial spectrum of MUSIC-like-FDB (ML-FDB) can be given as

$$P_{ML-FDB}(\theta) = \frac{1}{\|a_{Cum4}(\theta)E_n\|_1^2}. \quad (13)$$

The signal subspace dimension D significantly influences the performance of ML-FDB, which will be further analyzed later.

B. CA-FDB

Unlike the signal model of Cum4-FDB, CA-FDB needs first to calculate the second-order statistics. The cross correlation functions $R_{X_m X_1}(\tau)$ between X_m [defined in Eq. (7)] and X_1 can be given as

$$\begin{aligned} R_{X_m X_1}(\tau) &= E\{X_m(i)X_1^*(i + \tau)\} \\ &= E\left\{\left(\sum_{l=1}^p a_m^l S^l(i) + N_m(i)\right) \times \left(\sum_{k=1}^p a_1^k S^k(i + \tau) + N_1(i + \tau)\right)^*\right\} \\ &= E\left\{\sum_{l=1}^p a_m^l (a_1^l)^* S^l(i) (S^l(i + \tau))^* + \right. \\ &\quad \left. + E\left\{\sum_{l \neq k}^{p,p} a_m^l (a_1^k)^* S^l(i) (S^k(i + \tau))^*\right\}\right\} \\ &\quad + N_{R_m}(\tau). \end{aligned} \quad (14)$$

The second term is the cross term and can be ignored. The length of $R_{X_m X_1}(\tau)$ is $2N_f - 1$. Usually, $a_1^l = 1$, therefore, Eq. (14) can be rewritten as

$$R_{X_m X_1}(\tau) = \sum_{l=1}^p a_m^l R_{S^l S^l}(\tau) + N_{R_m}(\tau), \quad (15)$$

where

$$\begin{aligned} R_{S^l S^l}(j) &= E\{S^l(i)(S^l(i + \tau))^*\}, \\ N_{R_m}(\tau) &= E\left\{N_1^*(i + \tau) \sum_{l=1}^p a_m^l S^l(i)\right\} \\ &\quad + E\left\{N_m(i) \sum_{l=1}^p (a_m^l S^l(i + \tau))^*\right\} \\ &\quad + E\{N_1^*(i + \tau) N_m(i)\}, \end{aligned}$$

where N_m has been defined in Eq. (9). Equation (15) can be further written in matrix form

$$\begin{aligned} \mathbf{R}_X(\tau) &= \mathbf{A}\mathbf{R}_S(\tau) + \mathbf{N}_R(\tau), \\ \mathbf{R}_X(\tau) &= [R_{X_1 X_1}(\tau), R_{X_2 X_1}(\tau), \dots, R_{X_M X_1}(\tau)]^T, \\ \mathbf{R}_S(\tau) &= [R_{S^1 S^1}(\tau), R_{S^2 S^2}(\tau), \dots, R_{S^p S^p}(\tau)]^T, \\ \mathbf{N}_R(\tau) &= [N_{R_1}(\tau), N_{R_2}(\tau), \dots, N_{R_m}(\tau)]^T, \\ \mathbf{A} &= [a^1, a^2, \dots, a^p], \\ a^l &= \left[1, \exp\left\{-\frac{j2\pi d\Delta f \sin(\theta_l)}{c}\right\}, \dots, \right. \\ &\quad \left.\exp\left\{-\frac{j2\pi d(M-1)\Delta f \sin(\theta_l)}{c}\right\}\right]^T, \\ l &= 1, 2, \dots, p. \end{aligned} \quad (16)$$

Let

$$\begin{aligned} \mathbf{R}'_X(\tau) &= [R_{X_2 X_1}(\tau), R_{X_3 X_1}(\tau), \dots, R_{X_M X_1}(\tau)]^T, \\ \mathbf{A}' &= [a^1, a^2, \dots, a^p], \\ a'' &= \left[\exp\left\{-\frac{j2\pi d\Delta f \sin(\theta_l)}{c}\right\}, \dots, \right. \\ &\quad \left.\exp\left\{-\frac{j2\pi d(M-1)\Delta f \sin(\theta_l)}{c}\right\}\right]^T, \\ \mathbf{N}'_R(\tau) &= [N_{R_2}(\tau), \dots, N_{R_m}(\tau)]^T. \end{aligned} \quad (17)$$

a'' lacks the first element compared to a' , so the length is $M-1$. Take the conjugate of $\mathbf{R}'_X(\tau)$, and change τ to $-\tau$, we can get

$$\begin{aligned} (\mathbf{R}'_X(-\tau))^* &= (\mathbf{A}')^* \mathbf{R}_S^*(-\tau) + \mathbf{N}_R^*(-\tau) \\ &= (\mathbf{A}')^* \mathbf{R}_S(\tau) + (\mathbf{N}'_R(-\tau))^*. \end{aligned} \quad (18)$$

Combine Eqs. (16) and (18)

$$\mathbf{R}(\tau) = \begin{bmatrix} \mathbf{R}_X(\tau) \\ (\mathbf{R}'_X(-\tau))^* \end{bmatrix} = \begin{bmatrix} \mathbf{A} \\ (\mathbf{A}')^* \end{bmatrix} \mathbf{R}_S(\tau) + \begin{bmatrix} \mathbf{N}_R(\tau) \\ (\mathbf{N}'_R(-\tau))^* \end{bmatrix}. \quad (19)$$

Equation (19) is the broadband CA-FDB array signal model of one frame data and $\mathbf{R} \in \mathbb{C}^{(2M-1) \times (2N_f-1)}$.

When dealing with real data, $\mathbf{R}(\tau)$ will replace \mathbf{X} in Eq. (10) to calculate the Cum4 matrix and $\mathbf{C} \in \mathbb{C}^{(2M-1)^2 \times (2M-1)^2}$. The steering vector of CA-FDB is

$$\begin{aligned} \mathbf{a}_{CA}(\theta) &= \begin{bmatrix} a(\theta) \\ (a'(\theta))^* \end{bmatrix} \otimes \begin{bmatrix} a(\theta) \\ (a'(\theta))^* \end{bmatrix}^* \\ &= \begin{bmatrix} a(\theta) \otimes a^*(\theta) \\ a(\theta) \otimes a'(\theta) \\ (a'(\theta))^* \otimes a^*(\theta) \\ (a'(\theta))^* \otimes a'(\theta) \end{bmatrix}, \end{aligned} \quad (20)$$

where $a(\theta)$ has been defined in Eq. (11), and

$$\begin{aligned} a'(\theta) &= \left[\exp\left\{-\frac{j2\pi d\Delta f \sin(\theta_l)}{c}\right\}, \dots, \right. \\ &\quad \left.\exp\left\{-\frac{j2\pi d(M-1)\Delta f \sin(\theta_l)}{c}\right\}\right]. \end{aligned} \quad (21)$$

The length of $\mathbf{a}_{CA}(\theta)$ is $(2M-1)^2$. The DOA output of CA-FDB can be expressed as

$$P_{CA}(\theta) = \|\mathbf{a}_{CA}(\theta) \mathbf{C}\|^2. \quad (22)$$

Similar to the ML-FDB, the CA-FDB can also be combined with MUSIC (CAM-FDB) to achieve better performance.

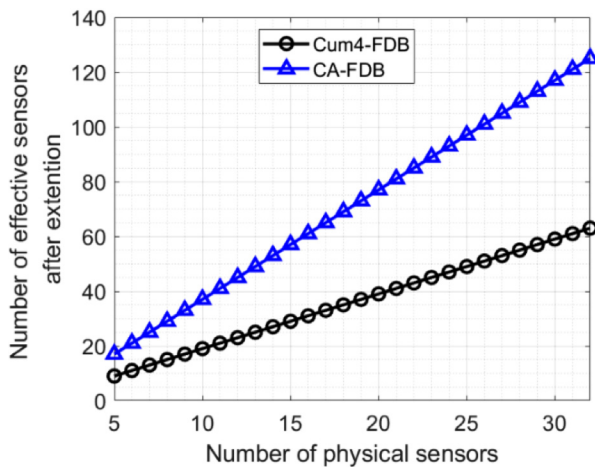


FIG. 1. (Color online) Number of effective elements after aperture expansion.

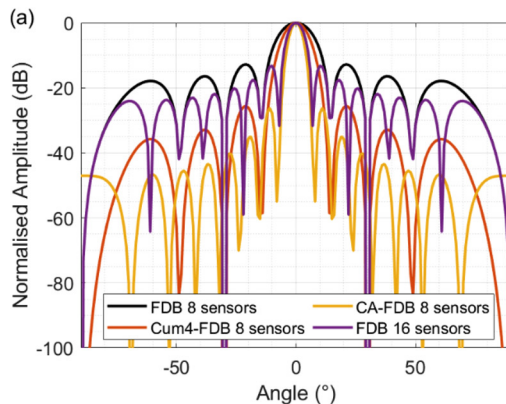
IV. SIMULATION ANALYSIS OF DOA PERFORMANCE

A. Effective aperture

Assuming that the position of each array element in an M -element uniform linear array is $D = [0, d_1, d_2, \dots, d_{M-1}]$, virtual elements will always be generated in Cum4-FDB according to the steering vector defined by Eq. (11), and the position is $-D$. However, there will be M elements overlapping at the 0, $M - 1$ elements overlapping at d_1 and $-d_1$, $M - 2$ elements overlapping at d_2 and $-d_2$, ..., and only one element at d_{M-1} and $-d_{M-1}$. Although $a_{\text{Cum4}}(\theta)$ is M^2 long, the effective element number is

$$\begin{aligned} M^2 - (M - 1) - 2*((M - 2) + (M - 3) + \dots + 2 + 1) \\ = 2M - 1. \end{aligned} \quad (23)$$

CA-FDB is similar. According to the steering vector defined in Eq. (20), $a(\theta_i) \otimes a^*(\theta_i)$ will obtain $2M - 1$ elements, similar to Cum4. Additionally, $a(\theta_i) \otimes a'(\theta_i)$ can obtain $M - 1$ new elements, and $(a'(\theta_i))^* \otimes a^*(\theta_i)$ can obtain another $M - 1$ new elements. Since $(a'(\theta_i))^* \otimes a'(\theta_i)$ is a subset of $a(\theta_i) \otimes a^*(\theta_i)$, no new element is obtained. Therefore, the CA-FDB can obtain a new aperture



consisting of $4M - 3$ elements. Figure 1 illustrates the effective element numbers after aperture expansion using the Cum4 and CA.

B. Beam width

For FDB output with difference frequency Δf , the normalized beam output of steering to direction θ_i is

$$BP_{FDB}(\sin \theta) = \left| \frac{\sin[M\pi\Delta fd(\sin \theta - \sin \theta_i)/c]}{M\sin[\pi\Delta fd(\sin \theta - \sin \theta_i)/c]} \right|^2, \quad (24)$$

while Cum4-FDB is

$$BP_{\text{Cum4}}(\sin \theta) = \left| \frac{\sin[M\pi\Delta fd(\sin \theta - \sin \theta_i)/c]}{M\sin[\pi\Delta fd(\sin \theta - \sin \theta_i)/c]} \right|^4, \quad (25)$$

CA-FDB,

$$BP_{CA}(\sin \theta) = \left| \frac{\sin[(2M - 1)\pi\Delta fd(\sin \theta - \sin \theta_i)/c]}{(2M - 1)\sin[\pi\Delta fd(\sin \theta - \sin \theta_i)/c]} \right|^4. \quad (26)$$

Figure 2(a) presents the normalized beam output when the sound source is located at 0° . The simulated arrays are uniform linear arrays with 8 and 16 elements, spaced at 1 m intervals, and the corresponding ideal signal frequency should be lower than 750 Hz. The simulated signal is a linear frequency modulation signal with a frequency range of 8~10 kHz and a pulse width of 0.1 s. Figure 2(b) presents the zoomed-in views. Table I lists the -3 dB main lobe width and highest sidelobe level. The CA-FDB method has the narrowest main lobe width, even narrower than the 16-element FDB array. Although the Cum4-FDB method can effectively reduce the main lobe width, its performance is less significant than the CA method. Both the Cum4-FDB and CA-FDB methods can reduce the sidelobe level by approximately 13 dB.

Figure 3 shows the DOA simulation results of two stationary incoherent sources at azimuths of -5° and 5° , with 8~10 kHz frequency bands. The results indicate that only the CA-FDB method can distinguish the two sources, while the

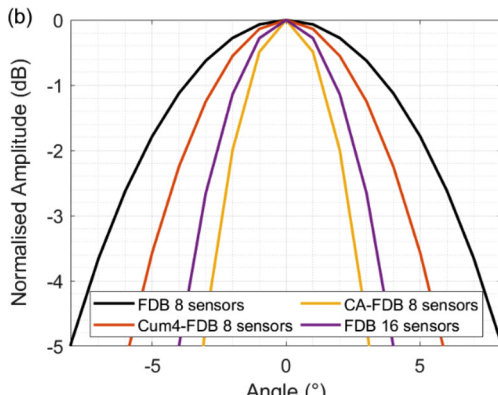


FIG. 2. (Color online) (a) Normalized beam output and (b) zoom view of the main lobes.

TABLE I. -3 dB main lobe width and highest sidelobe level.

	FDB 8 sensors	FDB 16 sensors	Cum4-FDB 8 sensors	CA-FDB 8 sensors
-3 dB main lobe width ($^\circ$)	11.26	6.29	9.14	4.76
Highest sidelobe level (dB)	-12.8	-13.2	-25.6	-26.3

FDB and Cum4-FDB methods cannot. The reason can be inferred from Eqs. (24)–(26). The beam output of Cum4-FDB is the square of FDB. Although it can effectively reduce the main lobe width, its theoretical angular resolution is consistent with that of the FDB. However, by combining MUSIC, the resolution of CUM4-FDB and CA-FDB can be further improved.

Combining the MUSIC algorithm to achieve higher resolutions requires careful selection of the signal subspace dimension D , which significantly affects the performance of MUSIC. Although it is suggested that the value of D should be equal to the square of the source number,¹⁰ it is not feasible in short arrays. We simulated an array with 8 elements, 1 m spacing, and two stationary targets with 8–10 kHz frequency bands. The simulation results indicate that FDB-MUSIC [Fig. 4(a)] is highly sensitive to the value of D . If D is smaller than the number of sources, some targets will be missed, and if D is too large, pseudo peaks will appear. The results also indicate that the performance of FDB-MUSIC is optimal when the number of sources is equal to D . The DOA performance of ML-FDB and CAM-FDB is more complicated, and it is best when D is set to 16 and 44, respectively, as shown in Figs. 4(b) and 4(c). Figure 4(d) compares the angular resolution obtained using the optimal D for ML-FDB and CAM-FDB. After selecting the proper D , both ML-FDB and CAM-FDB exhibit higher angular resolution, with the CAM-FDB method having the narrowest mainlobe and the lowest background level.

C. Weak target detection

FDB is known to struggle with detecting weak signals in the presence of strong interferers.³⁰ Real data processing

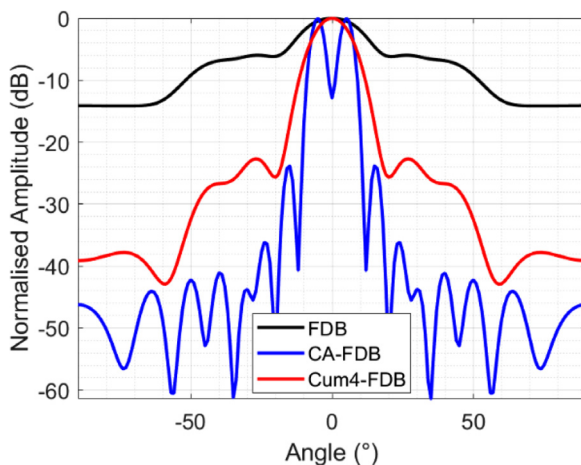


FIG. 3. (Color online) DOA result of two incoherent sources (-5° and 5°).

results also confirm this property and will be further demonstrated in Sec. V. Non-stationary sources like ships pose a greater challenge due to the fluctuation of the frequency-difference signals caused by changes in each frequency component. Nevertheless, we discovered that the weak target detection performance of ML-FDB and CAM-FDB is better than that of FDB and FDB-MUSIC when D is set appropriately. Figure 5 presents the DOA simulation results for two non-stationary sound sources (emitting Gaussian noise) using an array of eight elements spaced 1 m apart, a processing band of 8–10 kHz, and a difference frequency of 750 Hz. The weak target SNR was 10 dB lower than the strong target. Setting D to 30 and 150 resulted in accurate azimuth estimates of weak targets. FDB-MUSIC can also enhance the detection performance of weak targets by increasing D . However, compared with the two proposed methods in this study, FDB-MUSIC has limited adjustable D values (restricted by the number of array elements), and its DOA results are highly sensitive to D . Large D values can generate significant pseudo peaks, making it challenging to use FDB-MUSIC on short arrays. Although D was determined by pre-simulation when the array parameters are known in this paper, the selection of D deserves more in-depth research.

D. SNR requirement

The beamforming method based on Cum4 improves the array gain by suppressing noise. The Cum4 of Gaussian noise is 0, enabling the method based on Cum4 to suppress it. However, the noise of Cum4-FDB and CA-FDB becomes more complex after the frequency-difference calculations. The noise defined by Eqs. (9) and (19) contain complex conjugate products of signal and noise, as well as complex conjugate products of noise, which may impact the noise suppression performance of the Cum4. We simulated the DOA accuracy and array gain to evaluate the proposed methods' performance under noise influence. We simulated three 8–10 kHz stationary incoherent sound sources with azimuths θ_i at -30° , -10° , and 10° . D is set to 18 and 50 for ML-FDB and CAM-FDB. The root mean square error (RMSE) of the DOA estimations can be calculated by

$$RMSE = \sqrt{\sum_{i=1}^D (\theta_i - \hat{\theta}_i)^2}, \quad (27)$$

where $\hat{\theta}_i$ is the estimated value of θ_i .

The simulation results in Fig. 6(a) indicate that there is little difference in the SNR requirement between Cum4-FDB and the original FDB, suggesting that complex noise

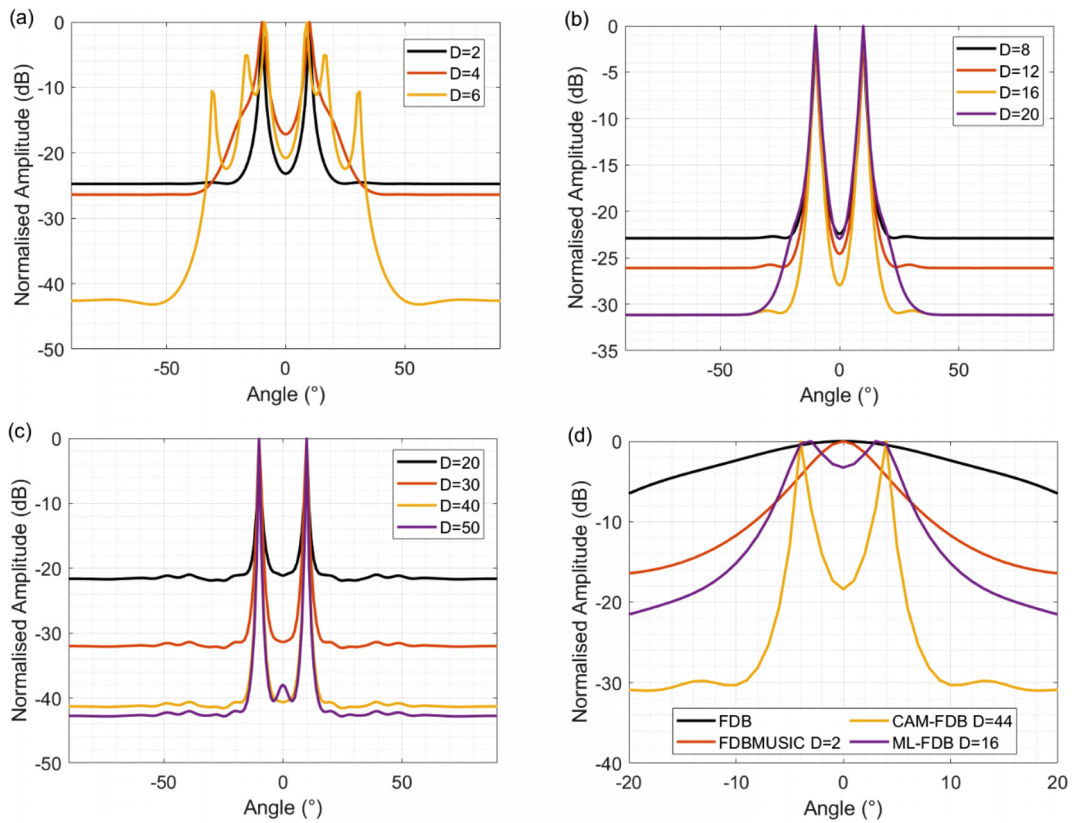


FIG. 4. (Color online) Influence of D on (a) FDB, (b) ML-FDB, (c) CAM-FDB. (d) Angular resolution when selecting the best D .

does affect the noise suppression performance of Cum4. We also included a comparison of the results for Deconv-FDB, which performed similarly to FDB. In contrast, the CA method appears to have some array gain, which is confirmed by the results in Fig. 6(b). Evidence of the array gain of CA-FDB was found in Ref. 27. Dogan demonstrated that by combining second-order statistics and fourth-order cumulants, non-Gaussian noise can be suppressed, and variation in the estimates can be reduced. However, this array gain is related to several factors, including the non-Gaussianity of

the sound source and noise and the data length. Therefore, giving a definite equation of the array gain is difficult.

E. Robustness to array geometry uncertainty

FDB is considered more robust to array geometry uncertainty than CBF because the transformation of signals into lower frequencies and variations in the array geometry affect both frequencies in a pair almost equally. We introduced a random position perturbation to the simulated array to analyze the proposed methods' robustness to array geometry uncertainty. Let the initial position of the array element be denoted by P ,

$$P = [(x_1, y_1), (x_2, y_2), \dots, (x_N, y_N)]. \quad (28)$$

The array element position error is given by

$$\Delta P = [(\Delta x_1, \Delta y_1), (\Delta x_2, \Delta y_2), \dots, (\Delta x_N, \Delta y_N)]. \quad (29)$$

Therefore, the actual array element position is expressed as

$$\tilde{P} = P + \Delta P. \quad (30)$$

The simulated array is an 8-element short array with 1 m spacing. The position errors, Δx and Δy , are assumed to follow a Gaussian distribution and can be adjusted by manipulating the standard deviation. A stationary sound source with azimuths of 0° and frequencies in the 8–10 kHz range is simulated. The average RMSEs are shown in Fig. 7.

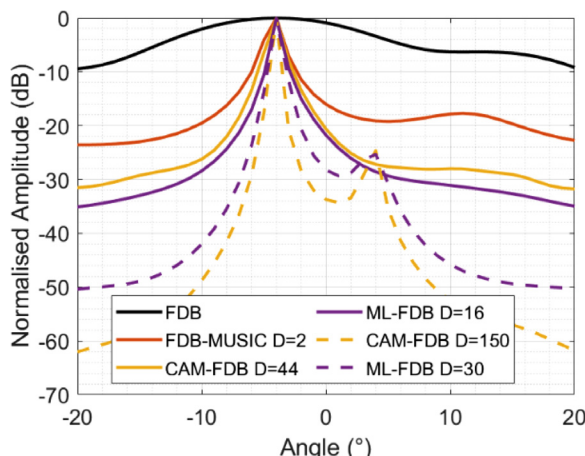


FIG. 5. (Color online) DOA estimation of weak non-stationary sources (-4° and 4°).

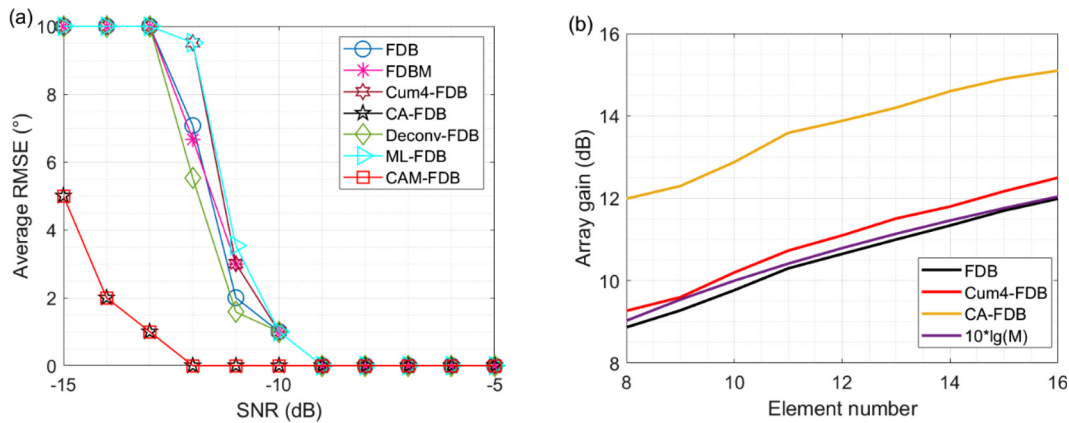


FIG. 6. (Color online) (a) DOA performance in different SNRs. (b) Array gain.

We found that Cum4-FDB and FDB exhibit similar levels of robustness, while the CA-FDB is less robust. A primary difference between Cum4-FDB and CA-FDB is that the CA method first needs to calculate the second-order statistics (cross correlation), which may amplify the uncertainty of array geometry. When the standard deviation of the array element position error is less than 5% of the array spacing, the difference in robustness is small and acceptable.

V. EXPERIMENT RESULTS

A. Case 1

The experiment was conducted in the South China Sea using a uniform horizontal array with a 6.25 m spacing, deployed at a depth of approximately 110 m. Only the first eight elements of the array were processed in this study. During the experiment, a power ship with its main engine turned on was moored near the array. The radiated noise created non-stationary interference to the experiment. Additionally, a towed sound source emitted signals between -20° and -10° , and a source of opportunity drove away from the array at around 15° . The array recorded the radiant

noise. Figure 8 presents a rough estimation of the SNR of the source of opportunity. As the target was obscured entirely by power ship interference in the time domain, we computed the target intensity and the background noise intensity using CBF, then subtracted the background noise intensity from the target intensity and further subtracted the array gain to obtain a rough estimate of the target's SNR. The SNR of self-ship interference varied between 3 dB and 4 dB, while the SNR of the active source was approximately 6 dB.

Each data frame has a length of 20 s and a sampling rate of 32 kHz. DOA estimates were computed every 1 s, and the 20 estimates were averaged to obtain the DOA result for each data frame. The processing band was set to 100~400 Hz, and a difference frequency of 100 Hz was selected. As mentioned in Sec. IV, the appearance of strong targets will reduce the detection performance of FDB on weak targets. This property is a common drawback of all FDB-based methods. Therefore, it can be found that when a strong target appears, it will decrease the intensity of other targets that appear simultaneously in Fig. 9. In Fig. 9(a), there are three faint lines in $[-30^\circ, 30^\circ]$ from the 1st to the 16th frame, these lines are not consistent with the target's orientation, and more like cross term interference or side

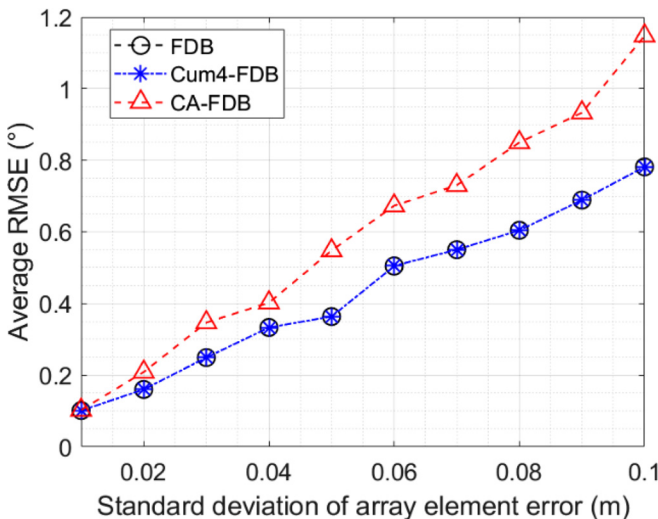


FIG. 7. (Color online) Robustness to array geometry uncertainty.

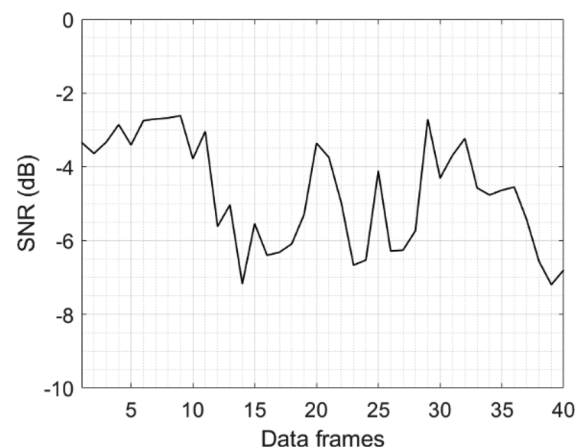


FIG. 8. The receiving SNR of the weak source of opportunity.

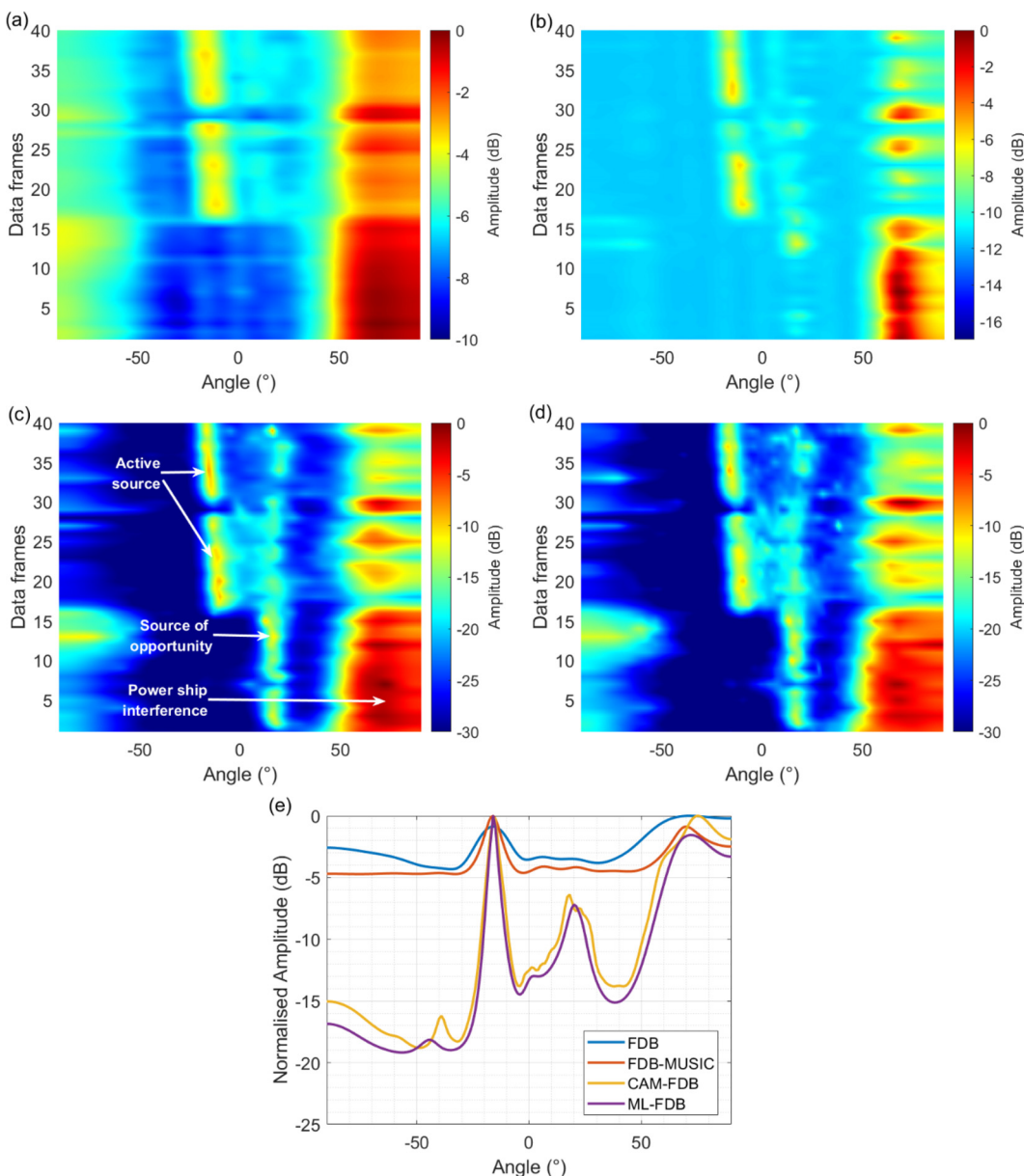


FIG. 9. (Color online) DOA results of (a) FDB, (b) FDB-MUSIC, (c) ML-FDB, and (d) CAM-FDB. The colorbars have been adjusted to better show the details of weak targets as much as possible. (e) DOA estimation of the 35th frame.

lobes. Similarly, the “targets” in 17~40 frames are mostly side lobes or cross-item interference generated by active sound sources, and it is difficult to distinguish the existence of weak targets. In Fig. 9(b), the weak target detection performance of FDB-MUSIC ($D = 3$) has been improved to some extent. The weak targets can be detected in some frames, such as 1~3 frames, 13~15 frames, etc., mostly because the self-ship interferences in these frames are relatively weak. In Figs. 9(c) and 9(d), 40 and 155 are selected as D values for ML-FDB and CAM-FDB, respectively, and all three targets are detected much clearer. However, the strong non-stationary interference still leads to the instability of weak targets. However, compared to FDB, this is already a significant improvement. Figure 9(e) shows the 35th frame result. The proposed algorithms not only detect

weak targets but also has a narrower main lobe width and lower background level.

B. Case 2

The second experiment evaluated the performance of the proposed methods in a coherent multi-path environment using a 6-element vertical array with a 10 m spacing. The experiment was conducted on the Chukchi Plateau in the Arctic, a marginal ice zone during summer. The local seabed has seamounts, and the depth varies between 800 and 1400 m. The sound source was placed at a depth of 102 m and emitted a chirp signal with a pulse width of 6 s and a frequency of 600~800 Hz once per minute. The first element of the vertical array was at a depth of 12 m, while the

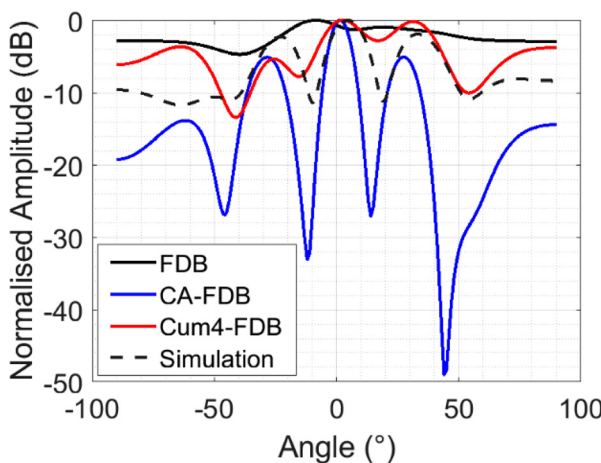


FIG. 10. (Color online) Average DOA results for 15 frames of data.

deepest was at 62 m. The distance between the sound source and the receiving array was around 800 m~1 km. A total of 15 data frames were collected.

Figure 10 shows the DOA results obtained by averaging 15 frames of data. Due to the coherent sound source, MUSIC was not used. A difference frequency of 70 Hz was selected, and the processing band was set to 600~800 Hz. To validate the data processing results, we conducted a scene reconstruction simulation based on the sound speed profile data and obtained the estimated DOA of the simulated multi-path arrivals. Compared to the original FDB, Cum4-FDB and CA-FDB achieved a more detailed and accurate estimation of the channel multi-path structure. CA-FDB had the narrowest mainlobe and lowest background level among them.

VI. DISCUSSIONS

Simulations and experimental results show that the two proposed methods yield narrow beams and low sidelobe levels than the original FDB on short, large-spacing arrays. Combining MUSIC, ML-FDB, and CAM-FDB achieved better angular resolution than the original FDB. CA methods have the narrowest mainlobe and are more adaptable to low SNRs due to the combination of second-order statistics. By setting the signal subspace dimension reasonably, ML-FDB and CAM-FDB can improve the weak target detection ability under strong interference compared with FDB. This advantage has been verified by real data of case 1. In case 2, Cum4-FDB and CA-FDB achieved a better performance in a coherent multi-path environment with only six elements. In addition, Cum4-FDB is consistent with the robustness of the array geometry uncertainty of FDB, while the robustness of CA-FDB is reduced. Yet/However its robustness is acceptable when the array geometry uncertainty is low. It is also worth mentioning that although the research in this paper is based on uniform linear arrays, the proposed methods are also applicable to non-uniform linear arrays.

Although the proposed methods have achieved good results, some details still need to be further studied in the

future. First, Due to the combination of the second-order statistics and the fourth-order cumulants, CA-FDB can improve the array gain of FDB. However, because of the complex influencing factors, it is difficult to give a definite equation of the array gain and needs further investigation.

Second, the signal subspace dimension D greatly affects the performance of ML-FDB and CAM-FDB. The choice of D needs to balance the detection performance of weak targets and the interference of pseudo peaks. Although D can be selected through pre-simulation, the relationship between the specific value of D and the number of sources and array elements is unclear.

Third, the computation complexity is the most significant disadvantage of Cum4-FDB and CA-FDB. Cum4-FDB needs to calculate the fourth-order cumulant to get a $M^2 \times M^2$ matrix and CA-FDB will generate a $(2M-1)^2 \times (2M-1)^2$ matrix. Therefore, the CA-FDB needs to adjust the length of the data frame and the number of FFT points according to the actual requirements to reduce the computation complexity.

Last, frequency-difference processing will generate undesired cross-terms. Although it did not affect the results in the data processing of this paper, it is unclear whether the cross-terms will change after the virtual aperture expansion.

As for the choice between the two methods, the CA methods would be better if the SNR is low, and the Cum4 methods can be used if lower computation complexity is required.

VII. CONCLUSIONS

This paper proposes two virtual aperture expansion methods based on fourth-order cumulants, Cum4-FDB and CA-FDB, to solve the problem of the low resolution of FDB on short arrays with large spacing. Cum4-FDB and CA-FDB expand the M -element uniform linear array to $2M-1$ and $4M-3$, respectively. Simulations and experimental results demonstrate that both algorithms produce narrower main lobes and lower sidelobe levels than FDB. Additionally, when combined with the MUSIC method, both algorithms can achieve higher angular resolution than FDB. The proposed methods can also improve the ability to detect weak targets under strong interference by setting the signal subspace dimension reasonably. However, the array gain of CA-FDB and the setting of the signal subspace dimension of the two algorithms still need further exploration.

ACKNOWLEDGMENTS

This research was funded by the National Natural Science Foundation of China (Grant No. U20A20329). The authors would also like to thank the editor and anonymous reviewer for their valuable comments on the rigor and completeness of the paper.

¹T. C. Yang, “Deconvolved Conventional Beamforming for a Horizontal Line Array,” *IEEE J. Oceanic Eng.*, **43**(1), 160–172 (2018).

- ²S. H. Abadi, D. Rouseff, and D. R. Dowling, “Blind deconvolution for robust signal estimation and approximate source localization,” *J. Acoust. Soc. Am.* **131**(4), 2599–2610 (2012).
- ³S. H. Abadi, H. C. Song, and D. R. Dowling, “Broadband sparse-array blind deconvolution using frequency difference beamforming,” *J. Acoust. Soc. Am.* **132**(5), 3018–3029 (2012).
- ⁴A. S. Douglass, H. C. Song, and D. R. Dowling, “Performance comparisons of frequency-difference and conventional beamforming,” *J. Acoust. Soc. Am.* **142**, 1663–1673 (2017).
- ⁵J. E. Lipa, B. M. Worthmann, and D. R. Dowling, “Measurement of auto-product fields in a Lloyd’s mirror environment,” *J. Acoust. Soc. Am.* **143**, 2419–2427 (2018).
- ⁶B. M. Worthmann and D. R. Dowling, “The frequency-difference and frequency-sum acoustic-field autoproduccts,” *J. Acoust. Soc. Am.* **141**(6), 4579–4590 (2017).
- ⁷A. S. Douglass and D. R. Dowling, “Frequency-difference beamforming in the presence of strong random scattering,” *J. Acoust. Soc. Am.* **146**(1), 122–134 (2019).
- ⁸B. M. Worthmann, H. C. Song, and D. R. Dowling, “High frequency source localization in a shallow ocean sound channel using frequency difference matched field processing,” *J. Acoust. Soc. Am.* **138**(6), 3549–3562 (2015).
- ⁹D. J. Geroski and D. R. Dowling, “Long-range frequency-difference source localization in the Philippine Sea,” *J. Acoust. Soc. Am.* **146**, 4727–4739 (2019).
- ¹⁰Y. Park, P. Gerstoft, and J.-H. Lee, “Difference-Frequency MUSIC for DOAs,” *IEEE Signal Process. Lett.* **29**, 2612–2616 (2022).
- ¹¹Y. Park, P. Gerstoft, and J.-H. Lee, “Difference-frequency MUSIC for beamforming,” *J. Acoust. Soc. Am.* **153**, A56 (2023).
- ¹²L. Xie, C. Sun, and J. Tian, “Deconvolved frequency-difference beamforming for a linear array,” *J. Acoust. Soc. Am.* **148**, EL440–EL446 (2020).
- ¹³P. Gerstoft, A. Xenaki, and C. F. Mechlenbräuker, “Multiple and single snapshot compressive beamforming,” *J. Acoust. Soc. Am.* **138**, 2003–2014 (2015).
- ¹⁴P. Gerstoft, C. F. Mecklenbräuker, W. Seong, and M. Bianco, “Introduction to compressive sensing in acoustics,” *J. Acoust. Soc. Am.* **143**(6), 3731–3736 (2018).
- ¹⁵J.-H. Lee, Y. Park, and P. Gerstoft, “Compressive frequency-difference direction-of-arrival estimation,” *J. Acoust. Soc. Am.* **154**(1), 141–151 (2023).
- ¹⁶G. S. Jo and J. W. Choi, “Subarray processing with coprime and minimum redundancy arrays,” *J. Acoust. Soc. Am.* **142**, 2523 (2017).
- ¹⁷S. Qin, Y. D. Zhang, and M. G. Amin, “Generalized coprime array configurations for direction-of-arrival estimation,” *IEEE Trans. Signal Process.* **63**, 1377–1390 (2015).
- ¹⁸C. Liu and P. P. Vaidyanathan, “Super nested arrays: Linear sparse arrays with reduced mutual coupling—Part I: Fundamentals,” *IEEE Trans. Signal Process.* **64**, 3997–4012 (2016).
- ¹⁹W.-K. Ma, T.-H. Hsieh, and C.-Y. Chi, “DOA Estimation of Quasi-Stationary Signals With Less Sensors Than Sources and Unknown Spatial Noise Covariance: A Khatri–Rao Subspace Approach,” *IEEE Trans. Signal Process.* **58**, 2168–2180 (2010).
- ²⁰C. Zhou, Y. Gu, Z. Shi, and Y. D. Zhang, “Off-grid direction-of-arrival estimation using coprime array interpolation,” *IEEE Signal Process. Lett.* **25**, 1710–1714 (2018).
- ²¹P. Gerstoft, C. F. Mecklenbräuker, A. Xenaki, and S. Nannuru, “Multisnapshot sparse Bayesian learning for DOA,” *IEEE Signal Process. Lett.* **23**, 1469–1473 (2016).
- ²²K. L. Gemba, S. Nannuru, P. Gerstoft, and W. S. Hodgkiss, “Multi-frequency sparse Bayesian learning for robust matched field processing,” *J. Acoust. Soc. Am.* **141**, 3411–3420 (2017).
- ²³G. Liang, C. Li, L. Qiu, T. Shen, and Y. Hao, “State-updating-based DOA estimation using sparse Bayesian learning,” *Appl. Acoust.* **192**, 108719 (2022).
- ²⁴M. Dogan, “Applications of cumulants to array processing. Part I. Aperture extension and array calibration,” *IEEE Trans. Signal Process.* **43**, 1200–1216 (1995).
- ²⁵P. Chevalier and A. Ferreol, “On the virtual array concept for the fourth-order direction finding problem,” *IEEE Trans. Signal Process.* **47**, 2592–2595 (1999).
- ²⁶Z. Shan and T.-S. P. Yum, “A conjugate augmented approach to direction-of-arrival estimation,” *IEEE Trans. Signal Process.* **53**, 4104–4109 (2005).
- ²⁷M. C. Dogan and J. M. Mendel, “Applications of cumulants to array processing. II. Non-Gaussian noise suppression,” *IEEE Trans. Signal Process.* **43**, 1663–1676 (1995).
- ²⁸D. J. Geroski and B. M. Worthmann, “Frequency-difference autoprodut cross-term analysis and cancellation for improved ambiguity surface robustness,” *J. Acoust. Soc. Am.* **149**(2), 868–884 (2021).
- ²⁹X. Wang, H. Sun, L. Zhang, C-p Dong, and L-x Guo, “Unambiguous broadband direction of arrival estimation based on improved extended frequency-difference method,” *J. Acoust. Soc. Am.* **152**(6), 3281–3293 (2022).
- ³⁰B. M. Worthmann, H. C. Song, and D. R. Dowling, “Adaptive frequency-difference matched field processing for high frequency source localization in a noisy shallow ocean,” *J. Acoust. Soc. Am.* **141**, 543–556 (2017).